Mechanistic basis for ubiquitin modulation of a protein energy landscape

Emma C. Carroll[a,1], Naomi R. Latorraca[a,1], Johanna M. Lindner[a], Brendan C. Maguire[b], Jeffrey G. Pelton[b], and Susan Marqusee[a,b,c,2]

[a]Department of Molecular and Cell Biology, University of California, Berkeley, CA 94720; [b]QB3 Institute for Quantitative Biosciences, University of California, Berkeley, CA 94720; and [c]Department of Chemistry, University of California, Berkeley, CA 94720

Edited by Lila M. Gierasch, University of Massachusetts Amherst, Amherst, MA, and approved February 8, 2021 (received for review December 7, 2020)

Ubiquitin is a common posttranslational modification canonically associated with targeting proteins to the 26S proteasome for degradation and also plays a role in numerous other nondegradative cellular processes. Ubiquitination at certain sites destabilizes the substrate protein, with consequences for proteasomal processing, while ubiquitination at other sites has little energetic effect. How this site specificity—and, by extension, the myriad effects of ubiquitination on substrate proteins—arises remains unknown. Here, we systematically characterize the atomic-level effects of ubiquitination at various sites on a model protein, barstar, using a combination of NMR, hydrogen–deuterium exchange mass spectrometry, and molecular dynamics simulation. We find that, regardless of the site of modification, ubiquitination does not induce large structural rearrangements in the substrate. Destabilizing modifications, however, increase fluctuations from the native state resulting in exposure of the substrate's C terminus. Both of the sites occur in regions of barstar with relatively high conformational flexibility. Nevertheless, destabilization appears to occur through different thermodynamic mechanisms, involving a reduction in entropy in one case and a loss in enthalpy in another. By contrast, ubiquitination at a nondestabilizing site protects the substrate C terminus through intermittent formation of a structural motif with the last three residues of ubiquitin. Thus, the biophysical effects of ubiquitination at a given site depend greatly on local context. Taken together, our results reveal how a single posttranslational modification can generate a broad array of distinct effects, providing a framework to guide the design of proteins and therapeutics with desired degradation and quality control properties.

ubiquitin | energy landscape | hydrogen exchange | molecular dynamics

Ubiquitin is an 8.5-kDa protein appended to target proteins as a posttranslational modification (PTM). Typically, ubiquitin is conjugated to the primary amine of substrate lysine residues, though noncanonical linkages to serine and cysteine also exist in vivo. Ubiquitin itself contains seven lysine residues, which allows building of ubiquitin chains with various linkages and topologies. Ubiquitination is most typically associated with targeting condemned proteins to the 26S proteasome for degradation; however, it is also involved in a large and ever-growing list of crucial regulatory, nondegradative cellular processes (1). A complex and highly regulated enzymatic cascade attaches ubiquitin to substrates and therefore plays a key role in determining the specific downstream effects of an individual ubiquitination event. There are several hundred E3 ligases, the terminal enzymes in this cascade (2), which give rise to broad proteome coverage and allow for some level of site specificity (3, 4).

Multiple different ubiquitin chain linkages and topologies bind with high affinity to proteasomal ubiquitin receptors and promote degradation (5–8). However, the presence of a ubiquitin tag alone is not sufficient to ensure proteasomal degradation. In fact, a substantial proportion of ubiquitin-modified proteins that interact with the 26S proteasome are ultimately released (9, 10) and not degraded. The proteasome also relies on substrate conformational properties, initiating degradation at an unstructured region on the condemned protein (11, 12). Much work has been done to understand the requirements of this unstructured region with regard to length, sequence composition, and topological position (13–15), yet at least 30% of known proteasome clients lack such a region (16). While evidence suggests that well-folded proteins are processed by diverse cellular unfoldases, such as Cdc48/p97/VCP (17, 18), an intriguing possibility is that the ubiquitin modification itself can modulate the conformational landscape and thus regulate proteasome substrate selection. Simulations have suggested that ubiquitination can destabilize the folded state of the substrate protein, thereby allowing it to more readily adopt unfolded or partially unfolded conformations (19, 20).

Recently, we demonstrated that this is indeed the case: ubiquitin can exert significant effects on a substrate's energy landscape depending on the site of ubiquitination and the identity of the substrate protein. Moreover, these changes can have direct consequences for proteasomal processing (21). By examining the energetic effects of native, isopeptide-linked ubiquitin attachment to three different sites within the small protein barstar from *Bacillus amyloliquefaciens*, we found that ubiquitin attached at either lysine 2 or lysine 60 destabilizes the protein both globally and via subglobal fluctuations, and we thus refer to these residues as sensitive sites. By contrast, ubiquitination at lysine 78 produces little effect on the energy landscape (21), and we therefore term it a nonsensitive site. Another study found that ubiquitin, appended through a nonnative linkage, can destabilize a folded substrate as

Significance

Fluctuations on a protein's energy landscape encode the mechanistic basis for vital biological processes not always evident from static structures alone. Ubiquitination, a key posttranslational modification, can affect a protein's energy landscape with consequences for proteasomal degradation, but the molecular mechanisms driving ubiquitin-induced energetic changes remain elusive. Here, we find that distinct thermodynamic mechanisms can produce the same outcome of ubiquitin-induced destabilization at sensitive sites. At a nonsensitive site, we observe formation of a substrate–ubiquitin interaction that may serve to protect against destabilization. This work will enable development of predictive models of the effect of ubiquitin at any given site on a protein with implications for understanding and engineering regulated ubiquitin signaling and protein quality control in vivo.

Author contributions: E.C.C., N.R.L., and S.M. designed research; E.C.C., N.R.L., J.M.L., B.C.M., and J.G.P. performed research; E.C.C., N.R.L., J.M.L., J.G.P., and S.M. analyzed data; and E.C.C., N.R.L., and S.M. wrote the paper.

The authors declare no competing interest.

This article is a PNAS Direct Submission.

[1]E.C.C. and N.R.L. contributed equally to this work.

[2]To whom correspondence may be addressed. Email: marqusee@berkeley.edu.

This article contains supporting information online at https://www.pnas.org/lookup/suppl/doi:10.1073/pnas.2025126118/-/DCSupplemental.

Published March 15, 2021.

measured by changes in the midpoints for thermally induced unfolding transitions (22).

Ubiquitination at the two sensitive sites in barstar increases the population of partially unfolded, high-energy states on the landscape sufficient for proteasomal engagement and degradation. Ubiquitination at the single nondestabilizing site does not allow for proteasomal degradation. These results suggest that ubiquitin-mediated destabilization can reveal an obligate unstructured region in substrates that otherwise lack such a region. Furthermore, ubiquitination at sensitive sites results in more rapid degradation of these barstar variants when a proteasome-engageable unstructured tail is fused to their C termini (21).

This previous work clearly demonstrates that ubiquitin-mediated changes to the protein landscape can play an important role in proteasomal selectivity and processing; it did not, however, uncover the molecular mechanisms through which these site-specific effects arise. Here, we interrogate the molecular mechanisms of ubiquitin-induced changes for these same single-lysine variants of barstar. We investigate differences in the intrinsic dynamics of these regions within barstar and differences in how the protein responds to ubiquitination at these individual sites. We employed two sets of complementary approaches: 1) NMR and HDX-MS (hydrogen–deuterium exchange mass spectrometry) to characterize the equilibrium conformational fluctuations of the substrate protein in the presence and absence of ubiquitin and 2) molecular dynamics (MD) simulations to track the position of every atom in barstar, in the presence and absence of ubiquitin, starting from its native conformation over the timescale of microseconds.

We find that ubiquitination has only subtle effects on the native structure of barstar. Ubiquitination at the sensitive sites, however, selectively increases fluctuations that expose barstar's C terminus. While both of the sensitive sites arise in regions of barstar with relatively high conformational flexibility, the observed destabilization appears to occur through different thermodynamic mechanisms. By contrast, ubiquitination at the nonsensitive site has a protective effect on barstar's C terminus. Thus, the effects of ubiquitination at each site are highly dependent on the local context. This mechanistic understanding of the site-specific effects of ubiquitination should aid in developing predictive models of the energetic consequences of individual ubiquitination events and also of the ways in which aberrant lysine targeting leads to disease (23–25).

Results

Monoubiquitination at all Three Sites Does Not Alter the Native Conformation of Barstar. As noted above, we previously characterized the energetic effects of ubiquitination at three distinct sites of the small protein barstar using single-lysine variants in which all but one native lysine had been mutated to arginine. Ubiquitination at positions K2 and K60 (the sensitive sites) destabilizes barstar ($\Delta\Delta G_{unfolding}$ ~2 and ~1.6 kcal/mol, respectively) as measured by equilibrium urea denaturation, while ubiquitination at K78 (the nonsensitive site) has essentially no effect. These energetic effects correlate with the observed changes in the population of partially unfolded states. Moreover, these changes allow for proteasomal engagement and degradation (21). We used these same single-lysine variants in this study (Fig. 1).

To determine whether ubiquitination alters the conformation of barstar, we first turned to NMR spectroscopy. Heteronuclear single quantum coherence (HSQC) NMR spectra were obtained for all three unmodified variants: barstarK2, barstarK60, and barstarK78 (Fig. 1). All three show very similar spectra that also closely resemble the published spectrum for wild-type barstar under slightly different conditions. Using the previously determined wild-type assignments (26, 27) and triple-resonance experiments, we assigned 69/88 barstar amides in unmodified barstarK60 to distinct peaks in the HSQC spectrum.

We next examined the HSQC spectra for the ubiquitin-modified variants. ^{15}N-labeled barstar variants were ubiquitinated with unlabeled, fully methylated ubiquitin [which increases yield of mono-ubiquitination and has been shown to induce the same energetic effects on barstar as nonmethylated ubiquitin (21)]. HSQC spectra reveal well-dispersed peaks characteristic of well-folded proteins (Fig. 1). Any ubiquitin-induced perturbations to the ground-state conformation appear to be relatively small for all three variants, as the HSQC of each ubiquitinated variant closely matches the HSQC of the corresponding unmodified variant (Fig. 1). These subtle effects are consistent with previous observations that, despite their destabilization and dramatic effects on proteasomal degradation, monoubiquitinated barstarK2 and barstarK60 unfold cooperatively and can still bind barstar's binding partner, barnase (21). For barstarK60, where we have assigned peaks, we observe notable changes in chemical shifts in the HSQC spectrum for residues directly surrounding the site of modification including E57, Q61, L62, and T63 (*SI Appendix*, Fig. S1*A*). These changes in chemical shifts may result from the presence of a nearby, covalently attached ubiquitin or from altered local behavior of the nearby residues upon ubiquitination.

In sum, these data indicate that all barstar variants adopt the native barstar-like fold in both their unmodified and mono-ubiquitinated states. In addition, an examination of barstar's structure (Protein Data Bank [PDB] 1BTA) reveals no obvious basis for the observed differences in stability across the three variants. For instance, local contact density in the vicinity of a given ubiquitination site does not correlate with the sensitivity of that site to ubiquitination (*SI Appendix*, Fig. S1*B*). The observed energetic and functional changes to barstarK2 and barstarK60 must therefore arise from shifts in the population of high-energy, partially or globally unfolded states on the landscape.

Conformational Flexibility in the Barstar Native State. To explore the mechanistic basis for the energetic differences observed upon ubiquitination, we first set out to characterize the conformational dynamics of unmodified barstar using complementary computational and experimental approaches. Do the regions containing sensitive sites (the K2 strand and K60 helix) differ in their conformational dynamics from the nonsensitive site (the K78 helix)?

We performed extensive all-atom MD simulations of unmodified barstar, starting from the conformation observed in the NMR structure, PDB 1BTA (27) (~30 μs in aggregate; see *Materials and Methods*). As expected, regions corresponding to portions of the sequence with secondary structure (α helices: residues 15 to 25, 34 to 43, and 68 to 80; and a β strand: residues 50 to 54) exhibit smaller backbone fluctuations compared to regions of the sequence lacking secondary structure (residues 7 to 14 and 25 to 33) (Fig. 2*A*).

Two exceptions to this general trend arise: in helix 3 (residues 55 to 63), which rapidly loses its initial helicity and adopts many loop-like conformations, and in strand 1 (residues 1 to 5), which occasionally separates from its neighboring strand. Notably, the sensitive sites (K60 and K2) map to these regions while the nonsensitive site (K78) does not. Additionally, throughout the course of each simulation, K2 and K60 form fewer contacts with neighboring residues compared to K78 (*SI Appendix*, Fig. S1). Thus, these simulations indicate that the two sensitive sites occur in regions of increased conformational flexibility relative to other regions of barstar with comparable secondary structure.

Experimentally, we evaluated the fluctuations in unmodified barstar using hydrogen–deuterium exchange monitored by NMR (HDX-NMR). ^{15}N-labeled barstarK60 was diluted into D_2O, and HSQC spectra were taken over a period of ~22 h. Using our amide backbone assignments, we followed the decrease in the individual amide proton intensity (peak volume) and calculated the observed exchange rate for a given amide (k_{obs}) (see *Materials and Methods*). From these rates, we then determined a protection factor, PF, using the known sequence-dependent exchange rates derived from

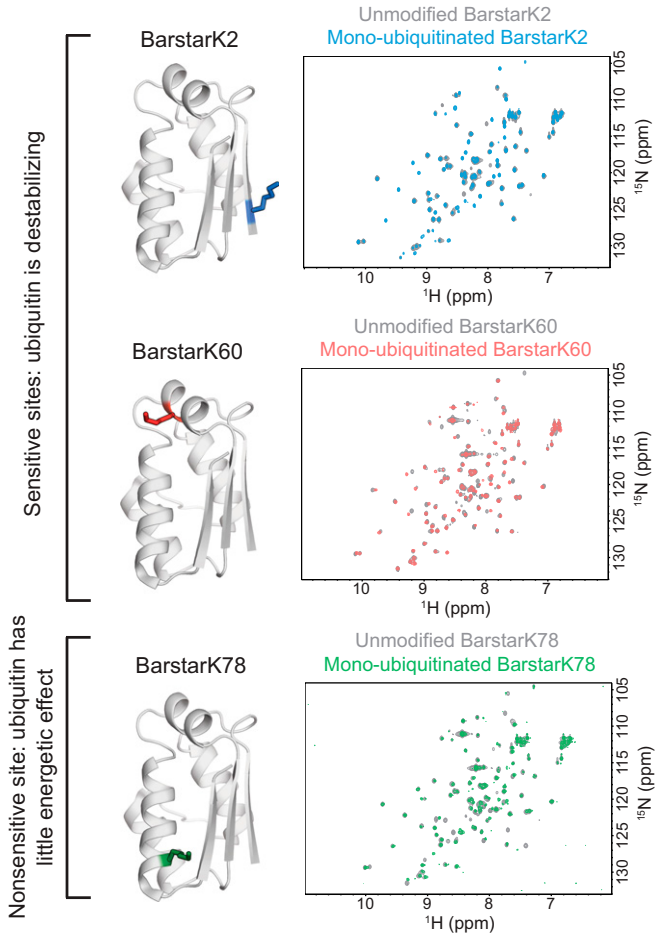

Fig. 1. Overview of barstar sensitive and nonsensitive ubiquitination sites and NMR HSQCs of unmodified and monoubiquitinated barstar variants. (*Left*) Ribbon diagrams (PDB 1BTA) depicting the position and surface topology of barstar lysine 2, a ubiquitin-destabilized site located in a β-strand, barstar lysine 60, a ubiquitin-destabilized site located in an α-helix, and barstar lysine 78, a site located in an α-helix that does not experience substantial destabilization upon ubiquitination. (*Right*) NMR ^{1}H/^{15}N HSQC spectra depict the chemical shifts of amides from each residue in unmodified (gray) and overlaid monoubiquitinated barstarK2 (blue), barstarK60 (red), and barstarK78 (green).

unstructured peptides, k_{rc} (28–30), in which PF = k_{rc}/k_{obs}. PF = 1 corresponds to a proton that exchanges at a rate expected for an unfolded amide, and PF > 1 corresponds to a protected amide. We successfully determined rates of exchange and the corresponding PFs for 38 of the 88 amide sites (Fig. 2*B*). In agreement with our simulations, most regions of secondary structure contained well-protected residues. Again, the primary exception is helix 3, which exhibited a notable lack of well-protected amides compared to the other helices in barstar.

Together, these simulations and experiments suggest that intrinsic dynamics, or flexibility, may be an important feature governing the effects of ubiquitination events at individual sites within a protein (Fig. 2*C*). They raise the possibility that sensitive sites may tend to occur within regions of high intrinsic flexibility, while nonsensitive sites may occur in regions of lower flexibility (see *Discussion*).

Ubiquitination at Sensitive Sites Alters Equilibrium Fluctuations. To characterize the changes in barstar equilibrium fluctuations upon ubiquitination, we again used hydrogen–deuterium exchange, this time monitored by mass spectrometry (HDX-MS), following exchange at the peptide level (see *Materials and Methods*). Despite providing lower resolution than HDX-NMR, HDX-MS yields a structural picture of the changes in dynamics and requires smaller amounts of sample such that the experiment is feasible with our monoubiquitinated barstar variants. We performed these experiments for all three unmodified and monoubiquitinated barstar variants and analyzed peptides from both barstar and ubiquitin. In these experiments, exchange was monitored over a time course of four to eight hours. Fig. 3 summarizes the results.

For all three variants, the majority of barstar peptides showed similar behavior in their ubiquitinated compared to unmodified states (Fig. 3*A* and *SI Appendix*, Fig. S2). Only a small number of peptides exhibit significant differences in deuterium uptake between unmodified and monoubiquitinated barstar (Fig. 3*B* and *SI Appendix*, Fig. S3). Both monoubiquitinated barstarK2 and barstarK60 show an increase in exchange compared to their unmodified counterparts that localizes to the C terminus and thus appears to rely on an allosteric network. This increased exchange,

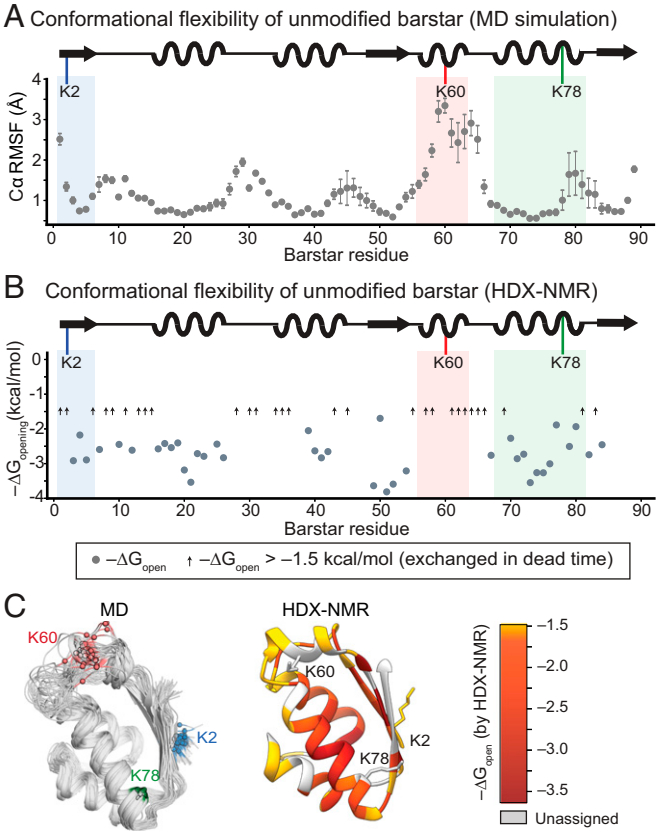

Fig. 2. Barstar sensitive sites exist within regions of high intrinsic conformational flexibility in the unmodified protein. (*A*) Sites sensitive to ubiquitination occur within relatively flexible regions of barstar, as measured by the RMSF (Å) of each Cα atom about its average position across six independent, 5.0-μs simulations of unmodified, wild-type barstar. Strand 1 (containing K2) is shaded in blue, helix 3 (containing K60) is shaded in red, and helix 4 (containing K78) is shaded in green. Error bars represent the SEM ($n = 6$). (*B*) Free energies of opening ($\Delta G_{opening}$) (gray circles) calculated from PFs obtained by HDX-NMR of unmodified barstarK60 and plotted by barstar residue number ($n = 1$). Amide residues that exchange faster than the 9.2-min dead time of the experiment are depicted by black arrows. Again, strand 1 (containing K2) is shaded in blue, helix 3 (containing K60) is shaded in red, and helix 4 (containing K78) is shaded in green. (*C*) Sites of backbone flexibility in barstar, as measured through MD and HDX-NMR. (*Left*) Overlapping simulation snapshots sampled every 100 ns after removing the first 1.0 μs (for equilibration) from a representative simulation of barstar. Spheres represent the Cα atom of each ubiquitination site. (*Right*) $\Delta G_{opening}$ values from HDX-NMR mapped onto the NMR structure of barstar (PDB 1BTA).

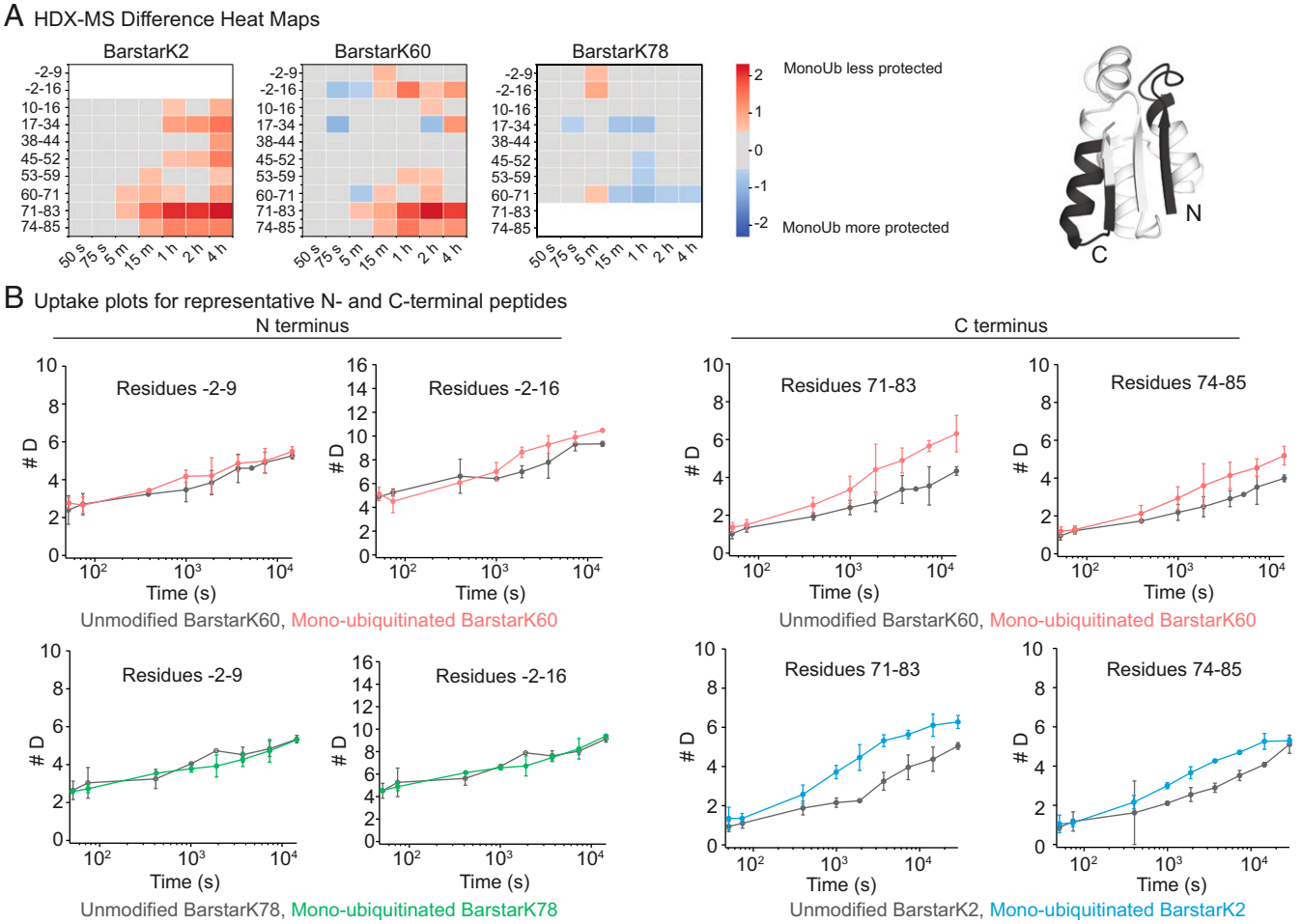

Fig. 3. Ubiquitination at sensitive sites on barstar destabilizes its C terminus. (*A*) Heat maps from representative peptides depicting differences in deuteration between unmodified and monoubiquitinated barstarK2, barstarK60, and barstarK78 ($n = 3$, barstarK2 and barstarK60; $n = 2$, barstarK78), from HDX-MS experiments. Red indicates increased deuterium exchange in the monoubiquitinated compared to the unmodified state, and blue indicates decreased deuterium uptake in the monoubiquitinated compared to unmodified state, both reported in Da. We consider a deuteration difference of at least ±0.5 Da between the unmodified and monoubiquitinated species meaningful and use gray squares to indicate points falling below this 0.5 Da limit. The barstar C terminus, but not its N terminus, becomes significantly destabilized upon ubiquitination at sensitive sites. Peptides containing the site of the modification could not be analyzed because the ubiquitin "scar" prevented accurate mass identification. Heat maps for the full peptide data sets are available in *SI Appendix*, Fig. S2. (*B*) Deuterium uptake plots not corrected for back exchange from representative peptides from the N- and C-terminal regions of unmodified (gray) and monoubiquitinated (blue) barstarK2, unmodified (gray) and monoubiquitinated (red) barstarK60, and unmodified (gray) and monoubiquitinated (green) barstarK78. Error bars represent the SD of replicates, and points are plotted at the average exchange time.

observed across multiple distinct C-terminal peptides in both barstarK2 and barstarK60, indicates a lower local stability upon ubiquitination. We could not analyze these same peptides for monoubiquitinated barstarK78 (the nonsensitive site) because the proteolysis scar (i.e., any ubiquitin residues still attached to the isopeptide bond) remaining from the ubiquitin modification prevented accurate peptide mass analysis/identification. At the N terminus, we do not observe any notable changes for barstarK60 and K78, which show nearly identical exchange profiles between unmodified and monoubiquitinated samples (Fig. 3*B*). Again, due to the ubiquitin scar, we could not analyze N-terminal peptides for monoubiquitinated barstarK2.

These changes at the C terminus are particularly intriguing because such flexibility may be responsible for the observed proteasomal processing of these destabilizing variants. For small proteasome substrates, the proteasome frequently engages at either terminus (12). Our previous biochemical evidence implicates the C terminus as the probable site of degradation initiation for barstarK2 (21).

Monitoring hydrogen exchange by mass spectrometry allows us to also follow peptides from ubiquitin, both in isolation and attached to barstar (See *Materials and Methods*). Interestingly, these peptides show no discernible change in extent or time course of exchange over the eight-hour experiment, indicating that any changes to ubiquitin are not detectable in this time window (*SI Appendix*, Fig. S4). This is surprising because, due to thermodynamic coupling, destabilization should be reciprocal. Nonetheless, ubiquitin possesses unusually high thermodynamic stability (31), and this high stability may serve to protect ubiquitin from unfolding and losing its signaling integrity upon conjugation to its myriad of targets in vivo (see *Discussion*).

Taken together, our HDX-MS and NMR analyses indicate that, while the three barstar variants all adopt the same native conformation, ubiquitination affects the conformational dynamics of each barstar variant differently. Specifically, the primary effects of ubiquitination at sensitive sites K2 and K60 occur in the C terminus, which experiences increased fluctuation upon ubiquitination. These results indicate that the effects of ubiquitination at these two sites propagate allosterically. The observed destabilization thus arises

from these changes in native-state dynamics rather than changes to the native structure, consistent with our previous studies that showed slow proteasomal degradation rates suggesting a required conformational fluctuation.

These HDX-MS experiments raise further mechanistic questions: if ubiquitin-induced destabilization primarily affects the flexibility and/or exposure of the substrate C terminus, how do modifications at sites far from the C terminus induce these effects? Conversely, how can a modification at a site within the C terminus, such as the nondestabilizing K78 modification, not destabilize the protein?

Thermodynamic Basis for Site-Specific Effects of Ubiquitination. To probe the molecular mechanism by which ubiquitination can site-specifically modulate the barstar conformational landscape, we again turned to MD simulations. For each barstar variant, we modeled an isopeptide bond to attach ubiquitin at the appropriate lysine site. Different potential lysine side-chain rotamers affect the orientation of ubiquitin with respect to barstar (*SI Appendix*, Fig. S5*A*). For each variant we selected the rotamer that maximized the distance between the centers of mass of barstar and ubiquitin (*SI Appendix*, Fig. S5*B*, see *Materials and Methods*). We then verified that simulations starting from these conformations could sample a wide variety of other conformations without becoming trapped in local minima, suggesting that the simulations are well-converged (*SI Appendix*, Fig. S6). For all three variants, the ubiquitin structure typically moves quickly with respect to barstar (*SI Appendix*, Fig. S6), and we only occasionally observe the formation of surface–surface interactions between the two proteins. All ubiquitinated variants sample fluctuations similar to those observed in simulations of unmodified barstar, with the secondary structure elements fluctuating less than regions composed of loops (*SI Appendix*, Fig. S7).

The most notable difference in conformational fluctuations occurs in monoUb-barstarK60, where residues within helix 3 (residues 55 to 68) displace less from their average position (i.e., fluctuate less) (Fig. 4*A* and *SI Appendix*, Fig. S7). A second difference occurs in the N terminus (residues 1 to 6) of monoUb-barstarK2, where residues 1 to 3 displace more from their average position (Fig. 4*B* and *SI Appendix*, Fig. S7). Importantly, within helix 3, monoUb-barstarK2 and monoUb-barstarK78 behave more similarly to unmodified barstar than to monoUb-barstarK60, and at the N terminus, monoUb-barstarK60 and monoUb-barstarK78 behave more similarly to unmodified barstar than to monoUb-barstarK2. Thus, our results indicate that ubiquitination at either of the two sensitive sites affects conformational fluctuations local to those sites, while ubiquitination at the nonsensitive site has little effect on local flexibility. We next set out to identify the atomic-level changes in barstar that underlie these observed changes in flexibility.

In simulations of monoUb-barstarK60, helix 3 samples a narrower range of conformations than it does in simulations of barstar alone or other monoubiquitinated variants. Specifically, its average simulated structure contains two full helical turns (*SI Appendix*, Fig. S8), and it fluctuates less about its average structure than do the other barstar variants (Fig. 4*A*). By contrast, and as described above, unmodified barstar often spontaneously samples nonhelical conformation, as does monoUb-barstarK2, and to a lesser extent, monoUb-barstarK78. Taken together, these results suggest that ubiquitin limits the number of conformations helix 3 samples when attached to K60 but not when attached at other sites. Thus, we propose that the substantial reduction in number of conformations sampled introduces an entropic penalty that destabilizes the native structure of barstar.

In simulations of monoUb-barstarK2, strand 1 separates from its neighboring strand more often than it does in simulations of barstar alone or other monoubiquitinated variants (Fig. 4*B*). In particular, it adopts conformations in which strand 1 forms fewer backbone–backbone hydrogen bonds with strand 2, thereby disrupting the beta sheet of barstar. Intriguingly, strand 1 occasionally separates from strand 2 across simulations of all variants, with and without ubiquitin; these excursions persist for longer periods of time in monoUb-barstarK2 (*SI Appendix*, Fig. S8). Moreover, a close examination of our simulations reveals that, for monoUb-barstarK2, the isopeptide linkage sometimes moves into the space between strand 1 and strand 2, thereby prolonging the amount of time monoUb-barstarK2 spends in this strand-displaced conformation. These observations are supported by our HDX-MS studies which show that peptides encompassing strand 2 undergo increased exchange in the monoUb-barstarK2 background (Fig. 3*A* and *SI Appendix*, Fig. S3). We therefore propose that ubiquitination at K2, but not at other sites, leads to direct disruption of the beta sheet in barstar, introducing an enthalpic penalty that destabilizes barstar.

In sum, these simulations indicate that while both sensitive sites arise in regions of local conformational flexibility, ubiquitination at each site induces destabilization through different molecular mechanisms, dominated by entropic effects (i.e., number of conformational states) in the case of K60 and by enthalpic effects (i.e., number of hydrogen bonds) in the case of K2. Importantly, the properties of the local conformational ensemble, rather than of the ground-state structure, appear to determine whether ubiquitin has an effect on each particular site. In each case, ubiquitination globally destabilizes the native state of barstar.

Notably, our simulations do not detect the concomitant exposure of the substrate C terminus observed in our HDX-MS experiments, likely because C-terminal exposure occurs on timescales associated with partial unfolding, which are beyond the scope of our simulations. Nevertheless, our data suggest that changes in the local flexibility near the two sensitive sites globally destabilize the native state of barstar, allosterically leading to increased exposure of the substrate C terminus.

How do these changes compare to the effects of ubiquitination at the nonsensitive site, K78? Across multiple independent simulations, monoubiquitinated barstarK78 samples a transient nonnative hydrogen bonding network between the C-terminal β strand of barstar and the flexible C terminus of ubiquitin (Fig. 5*A*), contributing an additional strand to the core β sheet of barstar. Moreover, the strand contributed by ubiquitin occludes the barstar C terminus, substantially reducing its solvent exposure in simulation (*SI Appendix*, Fig. S8*C*). These results provide an exciting molecular explanation for the lack of destabilization observed in this nonsensitive variant, and this increased stability at the C terminus may prevent barstarK78 from undergoing proteasomal degradation (21).

This nonnative hydrogen-bonding motif revealed in our simulations bears a striking resemblance to a motif observed in structures of a wide range of ubiquitin–protein binding interactions, including multiple classes of deubiquitinases (Fig. 5*B*). In all of these structures, the C-terminal tail of ubiquitin (typically residues 74 to 76) forms backbone–backbone hydrogen bonds with a β strand of the substrate protein (32–36). Thus, the isopeptide linkage, along with the local topology near the site of ubiquitination, facilitates specific interactions of ubiquitin with the substrate.

Aside from this nonnative hydrogen-bonding motif, long-lived, noncovalent interactions between barstar and ubiquitin form only rarely in simulation (*SI Appendix*, Figs. S6 and S9). Moreover, neither barstar nor ubiquitin exhibit regions of increased protection from hydrogen exchange in HDX-MS experiments of ubiquitinated variants. Global analysis of our simulations shows that long-range barstar–ubiquitin interactions occur with a frequency of at most ~20% of the time (*SI Appendix*, Fig. S9) and often involve the ubiquitin Ile44 surface hydrophobic patch, which has been extensively characterized as a ubiquitin–protein binding motif (37). Intriguingly, in the case of monoUb-barstarK2, ubiquitin occasionally adopts an orientation that allows its C terminus

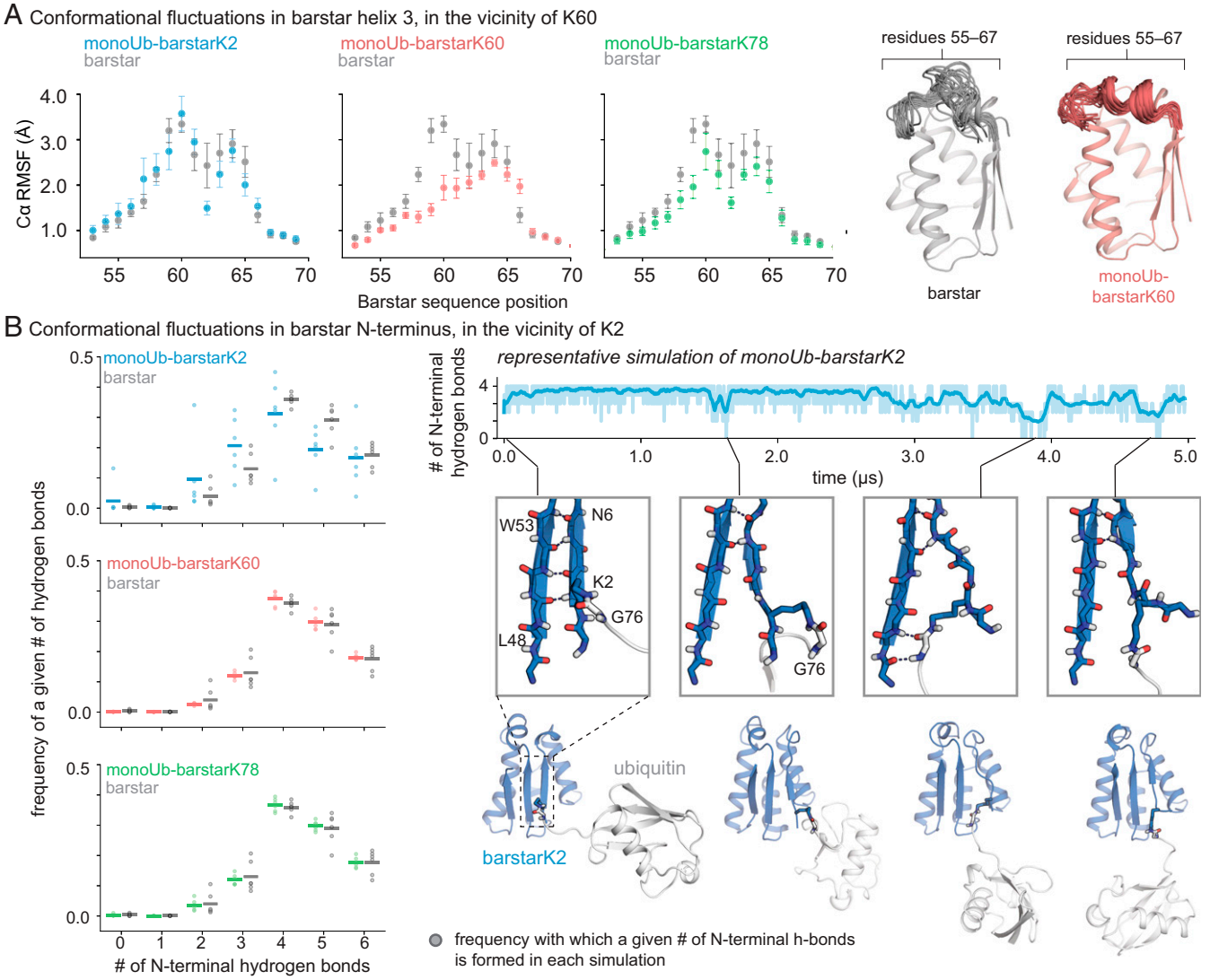

Fig. 4. Distinct thermodynamic mechanisms of ubiquitin-mediated destabilization in barstarK60 and barstarK2. (*A*) Ubiquitination of K60 reduces local conformational heterogeneity in the vicinity of the modification. Backbone fluctuations about the average structure, as measured by the RMSF of each Cα atom for the residues making up helix 3 (55 to 63). Error bars represent the SEM ($n = 6$ simulations per condition); within helix 3, differences in RMSFs between monoUb-barstarK60 and unmodified barstar are significant to $P < 0.005$, as measured with a Welch's two-sided t test, for Gln58, Ser59, and Lys60. On the right, simulation snapshots representing residues 55 to 67 of barstar sampled every 100 ns from a representative simulation are overlaid on the simulation starting structure. (*B*) Ubiquitination of K2 destabilizes interactions between the N-terminal β-strand of barstar and its neighboring β-strand (residues 50 to 53). For each simulation, we report the fraction of time a given number of hydrogen bonds forms between residues 1 to 5 and 48 to 54 (circles); mean values across a given condition depicted with horizontal bars. Ubiquitination at K2 increases the fraction of the time a simulation spends with three hydrogen bonds and decreases the fraction of the time a simulation spends with five hydrogen bonds compared to all other simulations (differences significant to $P < 0.05$ and $P < 0.001$, respectively, using a nonparametric rank sum test; see *Materials and Methods*). Thin trace (*Right*) shows the number of hydrogen bonds present between barstar strand 1 and strand 2 over time in a representative simulation. Thick trace represents a sliding average of simulation values smoothed over a 20-ns window. Ribbon diagrams illustrate conformations from the same simulation. In certain cases, ubiquitin's flexible C terminus occasionally forms intermittent nonnative hydrogen bonds with barstar strand 2 when strand 1 is displaced.

to move between strands 1 and 2 of barstar (Fig. 4*B*), raising the possibility that a particular ubiquitin orientation might contribute to its destabilizing effect at this modification site. However, the consequences of these transient barstar–ubiquitin surface interactions for ubiquitin's modulation of the barstar conformational landscape remain unclear from simulation alone.

Experimentally, we found that the "bulk" of ubiquitin does in fact appear to play a role in energetic changes upon ubiquitination. We took advantage of the recently re-engineered deubiquitinase LbPro*, which collapses ubiquitin modifications to only the C-terminal GG residues of the proximal ubiquitin, leaving an isopeptide-linked GG scar (38). We used a previously established native-state proteolysis assay in which the observed rate of proteolysis by thermolysin is directly related to the free energy of partial unfolding ($\Delta G_{proteolysis}$) (21, 39, 40). In this experiment, we find that LbPro*-treated monoUb-barstarK2 and monoUb-barstarK60 exhibit proteolysis kinetics intermediate between the monoubiquitinated and unmodified species (*SI Appendix*, Fig. S10). Therefore, the LbPro*-treated species are destabilized to a lesser degree than the monoubiquitinated variants but are still slightly destabilized compared to the unmodified species. Thus, simply modifying the two sensitive-site lysines is not sufficient to propagate the allosteric effects of ubiquitination; the full ubiquitin modification (or at least more of the bulk) is necessary to induce the full magnitude of the observed energetic changes.

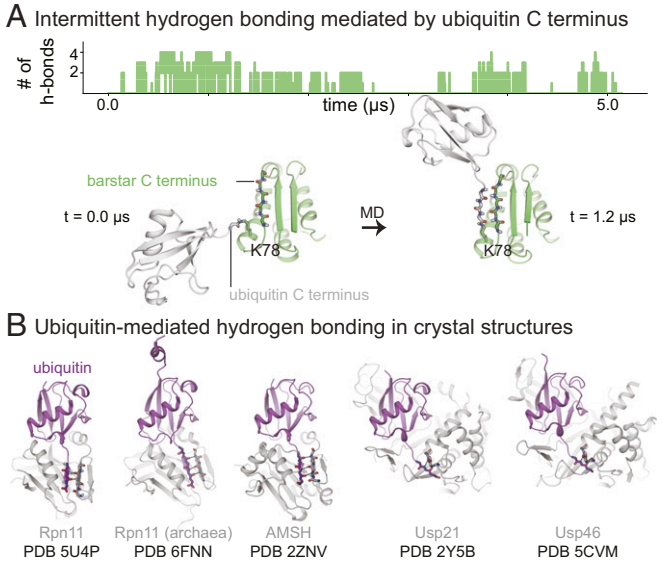

Fig. 5. Nonnative hydrogen bonding with ubiquitin's C terminus protects barstarK78's C terminus. (*A*) Ubiquitination at K78 protects the C-terminal β-strand of barstar, potentially stabilizing the substrate and protecting it from proteasomal targeting. Over the course of a simulation of barstar monoubiquitinated at K78, the ubiquitin C terminus forms transient hydrogen bonds with the C terminus of barstar. These hydrogen bonds occur consistently across all six independent simulations of K78-ubiquitinated barstar. (*B*) The ubiquitin C-terminal tail constitutes a protein recognition and binding site. Crystal structures of other ubiquitin-bound protein complexes also contain the same interaction motif observed in simulations of K78-ubiquitinated barstar.

Discussion

Using a combination of NMR, HDX-MS, and MD simulation, we interrogated the effects of site-specific ubiquitination on the conformational dynamics of barstar. Our results reveal site-specific mechanisms for ubiquitin-mediated changes. We find that these effects do not arise from changes in the ground-state structure of the substrate but rather are encoded by the substrate's energy landscape. Moreover, these mechanistic changes appear to underlie observed differences in proteasomal degradation. We find that modifications at sensitive sites allow barstar to populate partially unfolded states that expose its C terminus. Ubiquitination at the nonsensitive site allows the barstar C terminus to sample a potentially stabilizing interaction, as observed in simulation. The atomic-level changes associated with these effects arise from specific local properties of each modification site; for example, destabilizing effects can be dominated by either enthalpic contributions (i.e., by perturbing a substrate hydrogen bonding network) or entropic contributions (i.e., by reducing the number of configurations adopted by a region of the substrate).

We propose that, instead of dramatically changing the structure of the substrate, ubiquitin influences subglobal fluctuations on the energy landscape. This mechanism avoids the high energetic cost and potentially pathological consequences of fully unfolding a protein destined for degradation prior to its engagement with the 26S proteasome. These ubiquitin-induced modulations of the landscape allow the substrate to populate partially unfolded, high-energy conformation(s) sufficient for proteasomal engagement (21).

Our results suggest that ubiquitin induces fluctuations in the landscape that are either very sparsely populated or otherwise not accessible to the unmodified protein, thereby avoiding the population of substantially unfolded states that could template protein aggregation in cells. Thus, site-specific ubiquitin modulation might avoid aberrantly activating the protein quality control machinery or causing disease (41–44). In fact, previous studies have shown that the proteasome struggles to degrade aggregated proteins (45–47).

Due to thermodynamic coupling, barstar should reciprocally affect the energetics of ubiquitin. However, in our HDX-MS studies, we do not observe obvious barstar-induced effects on the landscape of ubiquitin. Our experiments only probe fluctuations within ~5 kcal/mol of the native state and, therefore, given the high stability of ubiquitin (~12 kcal/mol) (31), do not capture ubiquitin's global and large subglobal fluctuations. Ubiquitin's high stability may play an important role in providing tolerance and resistance to such energetic effects. Notably, ubiquitin has unusually high sequence conservation across multiple domains of life (48), but deep mutational scanning of ubiquitin has revealed its high tolerance to mutation (49, 50). Taken together, these results suggest that the stability of ubiquitin allows it to accommodate a range of perturbations, from a single-point mutation to covalent linkage with a similarly sized protein, without compromising its fold. We therefore propose that its unusually high stability may have evolved in order to protect ubiquitin from unfolding and thus from losing signaling recognition and integrity upon conjugation to its myriad targets in vivo.

Importantly, we demonstrate that the bulk of ubiquitin (i.e., residues other than just the isopeptide-linked C-terminal GG residues) contributes to its site-specific effects, but those effects do not appear to depend on the formation of specific protein–protein interaction surfaces. Ubiquitin has several surface motifs that mediate ubiquitin–protein binding interactions (51, 52). Although one of those "patches" formed occasional interactions with barstar in simulations of all three monoubiquitinated variants, neither experiments nor simulations identified surfaces of barstar or ubiquitin that became substantially protected in each other's presence. Nevertheless, native-state proteolysis experiments with LbPro*-treated barstarK2 and barstarK60 revealed that removing the bulk of ubiquitin partially ablated the destabilizing effect of ubiquitination. This observation is consistent with an "entropic pulling" effect, whereby transient interactions between the stably folded ubiquitin modification and substrate protein create a free energy gradient that generates a destabilizing net pulling force (53–55).

Critically, ubiquitin's site-specific effects depend on how its covalent attachment perturbs the local dynamics of the substrate surrounding a given site. These observations provide an explanation for how ubiquitination at many distinct sites, on a wide variety of substrates, can encode the same cellular fates. At each of the two sensitive sites, ubiquitin acts via distinct mechanisms to alter the flexibility of barstar and thereby reduce the population of the native conformation with a concomitant increase in the population of a proteasome-engageable partially unfolded state. Notably, the prediction that ubiquitination at K60 destabilizes the folded state through entropic destabilization makes sense in light of recent recognition that changes in the native state entropy can play an important role in the regulation of proteins (56) and computational studies on the effects of ubiquitination on substrate proteins (20). The ability of ubiquitin to modulate both the entropy and enthalpy of a system underscores its versatility as a PTM. More generally, previous protein engineering studies to stabilize proteins by increasing folded-state entropy have come with marked trade-offs in enzymatic function and protein activity (57). Thus, modulation of folded-state entropy by ubiquitination may have yet-unidentified effects on biological processes even at nondegradative ubiquitination sites (57, 58). At the nonsensitive site, ubiquitin's lack of effect correlates with the ability of its flexible C terminus to hydrogen bond with the barstar C terminus, contributing an additional strand to the barstar β sheet. Other substrates possessing a properly positioned, exposed set of backbone atoms might similarly interact with ubiquitin, also yielding protective effects. Interestingly, cocrystal structures of ubiquitin and various binding partners reveal similar structural motifs involving ubiquitin's C terminus. Thus, the

many conformational degrees of freedom of the native isopeptide bond, together with ubiquitin's flexible C-terminal tail, confer substrate and site specificity, and studies of ubiquitination that employ nonnative linkages may not capture such effects.

By extension, our results suggest that efforts to predict the effects of ubiquitination at a particular site need, at a minimum, to account for the conformational flexibility of the substrate and face considerable challenges. A handful of computational studies have sought to link structural properties of a ubiquitination site to ubiquitin's eventual effect. For example, a bioinformatics analysis revealed that, unlike phosphorylation sites, which primarily arise in disordered regions, ubiquitination sites can arise in both ordered and disordered regions (16). A subsequent study employing coarse-grained simulations found that high contact density in the vicinity of the ubiquitin modification negatively correlates with thermodynamic stability (19), which differs from our own observation that the two sensitive sites on barstar arise in regions of greater intrinsic flexibility. Thus, ubiquitination appears to exert specific effects at a given site through a variety of mechanisms.

Our own preliminary bioinformatic analysis based on the subset of known protein structures identified from a proteomic dataset of ubiquitinated substrates (59) (*SI Appendix*, Fig. S11) reveals that degradative and nondegradative ubiquitination sites are not readily distinguishable by the simple structural properties of the lysine residue such as its secondary structure, number of neighboring contacts, or its depth from the surface. With respect to ubiquitination sites identified within structured domains, our experimental and computational findings agree with and expand upon the results of these and other studies (20, 58); the effects of ubiquitination cannot be inferred from the static structure alone. Moreover, direct interactions between the substrate and ubiquitin may be highly dependent upon local geometric and structural features at each site (as in the predicted barstarK78–ubiquitin interaction). These potential ubiquitin–substrate interactions are neither easily inferred from bioinformatic approaches nor through examination of protein structures alone. Future mechanistic studies of the thermodynamic consequences of ubiquitination at individual sites are needed to bridge the current gap in predictive models. Developing the ability to predict the effect of ubiquitination at a given site on any given substrate will have implications for understanding how other cellular unfoldases that also recognize ubiquitinated proteins, such as p97, may respond to ubiquitin-induced energetic changes (17, 18) and, critically, in the design of therapeutics via targeted ubiquitination, such as PROTACs (60).

Although we have used several different biophysical approaches to interrogate the effects of ubiquitination in atomic-level detail, our study comes with several caveats. In our simulations, we have not captured the entire process by which local destabilization near the site of ubiquitination allosterically affects the substrate C terminus, enabling substrate unfolding. We have not probed detailed changes to the unfolded state; we expect those changes to take place on timescales longer than those sampled in our unbiased simulations. In our study, we employed two techniques—all-atom MD simulation and HDX-MS—that enable us to examine the native state and departures from the native state. Given that the proteasome does not require global unfolding for substrate engagement, these native-state fluctuations are likely to be responsible for the noted changes in proteasomal degradation (21). Additionally, we have only examined the effects of ubiquitination on a single protein substrate, barstar, and further work is required to expand our results to other proteins, particularly those with physiological degradative and nondegradative ubiquitination sites. Finally, we have only examined the mechanistic effects of monoubiquitination, and characterization of the effects of ubiquitin chains with diverse lengths, linkages, and topologies is needed to fully understand the energetic effects conferred by ubiquitination in vivo (61).

Taken together, our work supports the idea that site-specific ubiquitination events induce distinct and consequential mechanisms for modulating a protein's energy landscape. This site specificity allows a single PTM to have a broad range of effects in cells, a phenomenon also associated with phosphorylation and glycosylation (16, 62, 63). Site specificity of ubiquitin attachment is a built-in feature of the enzymatic conjugation and deubiquitination machinery in vivo, and the distinct mechanisms of ubiquitin-induced energetic effects represent an additional layer of protein quality control and signaling in cells.

Materials and Methods

Protein Purification of Unmodified Barstar Variants. Purified monoubiquitinated barstarK2, barstarK60, and barstarK78 were prepared as described in Ref. 21. Only barstar variants used in LbPro*-treated native-state proteolysis experiments were fluorescein-labeled.

Purification of Ubiquitination Enzymes. Ubiquitination enzymes *Mus musculus* E1, *Saccharomyces cerevisiae* Ubc4 E2, and *S. cerevisiae* Rsp5 E3 were purified as described in Ref. 21.

Purification of Ubiquitinated Barstar Variants. Purified monoubiquitinated barstarK2, barstarK60, and barstarK78 were prepared using methylated ubiquitin as described in Ref. 21 except that barstar variants were not fluorescein labeled (with the exception of those prepared for LbPro*-treated proteolysis experiments).

Purification of $^{15}N/^{13}C$-Labeled Proteins. *Escherichia coli* BL21 Rosetta 2 (DE3) cells were transformed with either pEC076 (barstarK2), pEC062 (barstarK60), or pEC059 (barstarK78). Cells were grown in M9 minimal media prepared with ^{15}N-labeled ammonium chloride as the sole nitrogen source. To prepare double-labeled samples, ^{13}C glucose was also included as the main carbon source. Cells were grown to $0.4 < OD_{600} < 0.8$ and induced with 1 mM IPTG overnight at 18 °C. Bacteria were pelleted and resuspended in 50 mM Hepes pH 7.0, 150 mM NaCl, and 0.5 mM TCEP supplemented with 1X Halt protease inhibitor mixture (Thermo Fisher) and benzonase (Novagen). Resuspended cells were lysed by sonication and the lysate was clarified by centrifugation at 20,000 rcf, 4 °C, 30 min. The substrate was first purified by Ni^{2+}-NTA affinity chromatography using its N-terminal His_6 tag. Clarified lysate was allowed to batch bind to HisPur Ni^{2+}-NTA resin (Thermo), washed with 50 mM Hepes pH 7.0, 150 mM NaCl, 25 mM imidazole, and 0.5 mM TCEP and eluted with 50 mM Hepes pH 7.0, 150 mM NaCl, 500 mM imidazole, and 0.5 mM TCEP. Eluate was then run over an S200 16/60 size exclusion column (GE) pre-equilibrated with 50 mM Hepes pH 8.0, 150 mM NaCl, and 5 mM $MgCl_2$. The peak corresponding to the full length His-MBP substrate was collected and quantified by ultraviolet-visible (UV-Vis) absorption at 280 nm before addition of 10% glycerol and flash freezing to store at −80 °C for future use.

Before NMR data acquisition, samples were thawed, cleaved with HRV3C protease overnight at 4 °C, and then run over an S75 16/60 size exclusion column (GE) equilibrated with 55 mM sodium phosphate, pH 6.5, and 55 mM NaCl to collect the pure unmodified barstar peak. Samples were concentrated to 250 μL for data collection in a Shigemi tube. Typical final sample concentrations were in the range of 0.75 to 2 mM (unmodified barstar) and 75 to 200 μM (monoubiquitinated barstar). Pure, monoubiquitinated ^{15}N-labeled barstar samples were purified using methylated ubiquitin as described in section 2.8.4. Samples were diluted with 10% D_2O before NMR data acquisition.

$^{15}N/^{1}H$ HSQC and $^{13}C/^{15}N/^{1}H$ HNCA and HNCACB NMR Data Acquisition and Processing. NMR experiments were recorded on a Bruker Inc. Avance II NMR spectrometer operating at 900 MHz and equipped with a Three Channel Inverse CryoProbe. The sample temperature was set to 298 K. Two-dimensional (2D) ^{1}H-^{15}N correlation spectra were recorded using the SOFAST heteronuclear multiple quantum coherence method (64) using Bruker pulse sequence sfhmqcf3gpph. A total of 2,048 and 256 pts were acquired in the ^{1}H and ^{15}N dimensions, respectively, with the ^{1}H offset centered at 8.3 ppm and the ^{15}N carrier frequency set to 120 ppm. The spectral widths were 16 ppm (^{1}H) and 40 ppm (^{15}N). The number of scans ranged from 4 to 32 depending on sample concentration, and the recycle delay was set to 0.5 s.

Three-dimensional (3D) HNCA and HNCACB spectra for unmodified barstarK60 were recorded using the T1 optimized BEST-HNCA (65, 66) and BEST-HNCACB (66) methods with Bruker pulse sequences b_hncagp3d and

bhncacbgp3d. For each experiment, a total of 1,024 (^{1}H), 64 (^{15}N), and 256 (^{13}C) pts were recorded with spectral widths of 14 ppm for ^{1}H and 35 ppm for ^{15}N. The ^{13}C spectral width was set to 40 ppm for the HNCA spectrum and 80 ppm for the HNCACB spectrum. A ^{1}H offset of 8.3 ppm was used, along with ^{15}N and ^{13}C carrier frequencies of 117.5 and 54 ppm, respectively. Four scans were signal averaged for each block, and the recycle delay was set to 0.5 s. Each spectrum was recorded in ~12 h. The 2D and 3D data were processed with the NMRPipe software package (67) and analyzed using Computer-Aided Resonance Assignment (CARA) (68).

^{15}N/^{1}H HSQC NMR Hydrogen–Deuterium Exchange. ^{15}N-labeled unmodified barstarK60 was run over an S75 10/300 size exclusion column (GE) equilibrated with 50 mM sodium phosphate pH 6.5 and 50 mM NaCl. The pure unmodified barstarK60 peak was collected and concentrated to 250 μL for eventual data collection in a Shigemi tube. The sample was then lyophilized overnight. The sample was resuspended in equivolume D_2O, and NMR data collection began immediately after redissolving the sample.

Amide proton exchange rates for unmodified barstarK60 were obtained by measuring intensities of peaks in a series of 2D ^{1}H-^{15}N correlation spectra recorded using the SOFAST-HMQC (64) method. For each spectrum, eight scans were signal averaged per block, resulting in an acquisition time of 20 min. Sixteen spectra were recorded with initial time points of 9.2, 30.1, 50.9, 71.7, 92.5, 113.3, 134.1, 154.9, 175.7, 196.5, 217.3, 255.6, 516.4, 777.2, 1,037.9, and 1,298.8 min after dissolution of lyophilized protein into D_2O.

HDX-MS. To prepare deuterated buffer, 5 mL of a 50 mM Hepes pH 7.0, 50 mM NaCl, 50 mM KCl, and 10 mM $MgCl_2$ buffer was lyophilized overnight. The lyophilized buffer was then resuspended in equivolume D_2O and allowed to exchange for 6 h at room temperature and relyophilized. This process was repeated for a total of three D_2O resuspension and lyophilization steps. The lyophilized buffer was stored at −80 °C.

All three unmodified and all three monoubiquitinated barstar variants were purified via size-exclusion chromatography as described above and then diluted with 50 mM Hepes pH 7.0, 50 mM NaCl, 50 mM KCl, and 10 mM $MgCl_2$ buffer to a final concentration of 10 μM in preparation for mass spectrometry (MS) experiments described below.

All HDX-MS experiments were performed using a liquid handling robot (LEAP Technologies) connected to a Q Exactive mass spectrometer (Thermo Fisher). The liquid handling robot was programmed to initiate amide proton exchange at 20 °C by diluting barstar or monoubiquitinated barstar to 1 μM into deuterated buffer (50 mM Hepes, pH 7, 50 mM NaCl, 50 mM, KCl, and 10 mM MgCl2) and then quenching exchange at various timepoints by adding low-pH buffer (6 M urea, 200 mM Arginine, 100 mM TCEP, and pH 2.5) and cooling to 1 °C. Quench buffer was added to the exchanging sample in a 1:1 ratio by volume such that the final protein concentration = 0.5 μM. The liquid handling robot was programmed to collect time points at 30, 60, 300, 900, 1,800, 3,600, 7,200, 14,400, and 28,800 s; however, actual quench times are reported as source data. Average quench times for each programmed time point are used in Fig. 3*B*. After quenching, the samples were directly subjected to an in-line proteolysis step using one pepsin-packed column (barstar peptides) or one pepsin followed by one fungal protease-packed column (ubiquitin peptides). Proteolysis was followed directly by liquid chromatography using a C4 trap column followed by a C8 analytical column eluted with a 10 to 100% acetonitrile gradient and identified via MS. Peptide lists were generated from an MS/MS run performed on each replicate using either Proteome Discoverer (Thermo Fisher) or Byonic (Protein Metrics). For methylated sites, only peptides containing the dimethylation modification were analyzed. Peptide deuteration states and isotopic distributions were then determined using HDExaminer 2 (Sierra Analytics) with manual adjustment to the HDExaminer peak identifications as needed. Data are reported as absolute mass increases (comparing unmodified and monoubiquitinated variants to one another within the same experiment) and are not corrected for back exchange.

To construct difference heat maps, absolute mass values for the unmodified variants were subtracted from absolute mass values for the modified variants at each time point. We performed the subtraction on experiments of the unmodified and modified variants taken on the same day and then averaged the resulting difference values. We do not consider differences less than ±0.5 Da as meaningful; those data points are colored gray in the heat maps (69). Additionally, we excluded peptides greater than 20 residues in length.

Purification of LbPro*. The gene encoding LbPro* (38) was cloned into an expression vector with an N-terminal, HRV3C protease–cleavable His-MBP tag to create pEC129. *E. coli* BL21 (DE3) cells were transformed with pEC129 and grown in Luria–Bertani media to $0.4 < OD_{600} < 0.8$ and induced with 1 mM IPTG at 37 °C for 3 h. Bacteria were pelleted and resuspended in 50 mM Hepes pH 7.5, 150 mM NaCl, and 0.5 mM TCEP supplemented with 1X Halt protease inhibitor mixture (Thermo Fisher) and benzonase (Novagen). Resuspended cells were lysed by sonication and the lysate was clarified by centrifugation at 20,000 rcf, 4 °C, 30 min. The construct was purified by Ni^{2+}-NTA affinity chromatography using its N-terminal His_6 tag. Clarified lysate was allowed to batch bind to HisPur Ni^{2+}-NTA resin (Thermo Fisher) washed with 50 mM Hepes pH 7.5, 150 mM NaCl, 25 mM imidazole, and 0.5 mM TCEP and eluted with 50 mM Hepes pH 7.5, 150 mM NaCl, 500 mM imidazole, and 0.5 mM TCEP. Eluate containing pure protein was then concentrated and quantified by UV-Vis absorption at 280 nm before addition of 10% glycerol and flash freezing to store at −80 °C for future use. Retention of the N-terminal His-MBP tag did not affect enzymatic processing, as whole-protein MS confirmed that deubiquitination reactions yielded a ubiquitin species lacking the C-terminal GG residues.

LbPro* Deubiquitination and Native-State Proteolysis Experiments. Purified, monoubiquitinated samples prepared with methylated ubiquitin and labeled with fluorescein-maleimide on the single cysteine at position 82 were treated with 20 μM LbPro* at 37 °C for 1 h in reaction buffer (25 mM Hepes pH 7.5, 150 mM KCl, and 15 mM MgOAc) supplemented with 2 mM dithiothreitol. LbPro* treatment generated a mixed population of monoubiquitinated and GG-modified barstar. Samples were then batch bound with amylose resin to remove the His-MBP–LbPro* enzyme, and the flow through was collected. Samples were allowed to equilibrate back to room temperature overnight, and then native-state proteolysis experiments were performed with 0.2 mg/mL thermolysin protease (Sigma-Aldrich). Time points were taken a t = 0, 0:15, 0:30, 0:45, 1:00, 1:30, 2:00, 3:00, 5:00, 7:00, and 10:00 min and quenched with EDTA. Each time point was then run on a NuPAGE Bis-Tris gel (Invitrogen) and band intensities quantified using ImageJ. Proteolysis rates are proportional to the free energy of partial unfolding to the protease-cleavable state ($\Delta G_{proteolysis}$) and have been previously measured for unmodified and monoubiquitinated barstarK2, barstarK60, and barstarK78 (21).

MD Simulations. We simulated barstar under four conditions: on its own and with a single monomer of ubiquitin covalently attached, via an isopeptide linkage, to one of three sites on barstar (K2, K60, and K78). We initiated simulations of barstar alone from the NMR structure of barstar, PDB entry 1BTA (27). To model each monoubiquitinated variant we employed the crystal structure of ubiquitin, PDB entry 1UBQ (70). In order to place ubiquitin near to its site of attachment, we aligned the lysine side chain to the ubiquitin-linked lysine side chain K48 in chain B of PDB entry 3NS8 and the ubiquitin C-terminal glycine of 1UBQ to the corresponding atoms in chain A of 3NS8. We used Maestro (Schrödinger, Inc.) to form an isopeptide bond between the lysine side-chain nitrogen atom and the glycine carbonyl carbon and selected the lysine rotamer that maximized the distance between the centers of mass of ubiquitin and barstar. We prepared the resulting structures in Maestro, retained titratable residues in their dominant protonation state at pH 7, and added neutral groups to cap the free N and C termini.

Prepared proteins were placed in a water box using LEaP in AMBER (71), resulting in boxes with initial dimensions of 75 Å × 75 Å × 75 Å for barstar alone and 102 Å × 102 Å × 102 Å for each mono-ubiquitinated barstar. We also used Dabble (72) to guide generation of input files for LEaP. We used the AMBER ff14SB force field for protein atoms, the TIP3P parameter sets for ions, and the TIP4P-D model for waters (73–75).

We performed six independent ~5 μs simulations for each construct using AMBER18 on single graphical processing units (71, 76). See *SI Appendix* for a complete description of model building and simulation protocols.

Analysis of Ubiquitination Sites Identified by Proteomics Screen. To determine whether sites of ubiquitination, within structured protein regions, differ in their local properties depending on whether they encode either degradative or regulatory effects, we analyzed a mass spectrometry dataset from ref. 59. These data represent the 200 most abundant sites for which spectral counts of di-glycine-glycine (dGG)-containing peptides changed by more than twofold upon proteasomal inhibition by epoxomicin. Sites were categorized as "degradative," if they increased in abundance upon inhibition, or "regulatory," if they decreased in abundance upon inhibition. Uniprot IDs corresponding to proteins containing dGG sites were mapped to their entries in the Protein Data Bank using the Retrieve ID/mapping tool in Uniprot (https://www.uniprot.org/uploadlists/). We employed Biopython (77) to select the lysine residue within a PDB that corresponded to the ubiquitin modification site specified in the

dataset above. For each site present within a PDB structure, we used mkDSSP [https://slackbuilds.org/repository/14.1/academic/mkDSSP/ (78)] to classify its secondary structure as well as its relative accessible surface area (rASA). For each ubiquitination site, we selected one representative PDB to determine the depth of each lysine side chain from the surface [mgltools.scripps.edu/packages/MSMS (79)] and the number of residues within 4.5 Å of any nonhydrogen side-chain atom.

Data Availability. Peak assignments from HSQC NMR spectra have been deposited in the Biological Magnetic Resonance Data Bank (ID: 50539). Peak integrations and PF calculations for the HDX-NMR data, raw HDX-MS data (deuterium uptake measurements over time), downsampled simulation trajectories, and simulation metadata and analysis code have been uploaded to Zenodo (http://doi.org/10.5281/zenodo.4489995). All other study data are included in the article and/or supporting information.

ACKNOWLEDGMENTS. We thank all members of the Marqusee laboratory for helpful discussions and scientific guidance. We thank Helen Hobbs, Robin Betz, Robert Best, Andy Martin, Greg Bowman, Carl-Mikael Suomivuori, Ken Dong, and Meredith Rickard for helpful advice and feedback. We also thank Jeff Morrow and Sierra Analytics for making HDExaminer licenses freely available for at-home use during shelter-in-place orders, and Berkeley Research Computing for providing computational resources through the Savio cluster. This work was supported by the US NIH R01GM050945 to S.M. S.M. is a Chan Zuckerberg Biohub Investigator. N.R.L. is a University of California, Berkeley, Miller Fellow. Funds for the 900 MHz NMR spectrometer were provided by the NIH through grant GM68933.

1. D. Komander, M. Rape, The ubiquitin code. *Annu. Rev. Biochem.* **81**, 203–229 (2012).
2. L. K. Nguyen, Dynamics of ubiquitin-mediated signalling: Insights from mathematical modelling and experimental studies. *Brief Bioinform.* **17**, 479–493 (2016).
3. V. K. Chaugule, H. Walden, Specificity and disease in the ubiquitin system. *Biochem. Soc. Trans.* **44**, 212–227 (2016).
4. N. Zheng, N. Shabek, Ubiquitin ligases: Structure, function, and regulation. *Annu. Rev. Biochem.* **86**, 129–157 (2017).
5. I. Livneh, Y. Kravtsova-Ivantsiv, O. Braten, Y. T. Kwon, A. Ciechanover, Monoubiquitination joins polyubiquitination as an esteemed proteasomal targeting signal. *BioEssays* **39**, 1–7 (2017).
6. Y. Kravtsova-Ivantsiv, T. Sommer, A. Ciechanover, The lysine48-based polyubiquitin chain proteasomal signal: Not a single child anymore. *Angew. Chem. Int. Ed. Engl.* **52**, 192–198 (2013).
7. Y. Lu, B.-H. Lee, R. W. King, D. Finley, M. W. Kirschner, Substrate degradation by the proteasome: A single-molecule kinetic analysis. *Science* **348**, 200–211 (2015).
8. G. L. Grice, J. A. Nathan, The recognition of ubiquitinated proteins by the proteasome. *Cell. Mol. Life Sci.* **73**, 3497–3506 (2016).
9. A. Peth, T. Uchiki, A. L. Goldberg, ATP-dependent steps in the binding of ubiquitin conjugates to the 26S proteasome that commit to degradation. *Mol. Cell* **40**, 671–681 (2010).
10. G. A. Collins, A. L. Goldberg, The logic of the 26S proteasome. *Cell* **169**, 792–806 (2017).
11. S. Prakash, L. Tian, K. S. Ratliff, R. E. Lehotzky, A. Matouschek, An unstructured initiation site is required for efficient proteasome-mediated degradation. *Nat. Struct. Mol. Biol.* **11**, 830–837 (2004).
12. T. Tomita, A. Matouschek, Substrate selection by the proteasome through initiation regions. *Protein Sci.* **28**, 1222–1232 (2019).
13. D. Berko *et al.*, The direction of protein entry into the proteasome determines the variety of products and depends on the force needed to unfold its two termini. *Mol. Cell* **48**, 601–611 (2012).
14. S. Fishbain *et al.*, Sequence composition of disordered regions fine-tunes protein half-life. *Nat. Struct. Mol. Biol.* **22**, 214–221 (2015).
15. J. A. M. Bard, C. Bashore, K. C. Dong, A. Martin, The 26S proteasome utilizes a kinetic gateway to prioritize substrate degradation. *Cell* **177**, 286–298.e15 (2019).
16. T. Hagai, A. Azia, Á. Tóth-Petróczy, Y. Levy, Intrinsic disorder in ubiquitination substrates. *J. Mol. Biol.* **412**, 319–324 (2011).
17. D. Gödderz *et al.*, Cdc48-independent proteasomal degradation coincides with a reduced need for ubiquitylation. *Sci. Rep.* **5**, 7615 (2015).
18. M. M. Olszewski, C. Williams, K. C. Dong, A. Martin, The Cdc48 unfoldase prepares well-folded protein substrates for degradation by the 26S proteasome. *Commun. Biol.* **2**, 29 (2019).
19. T. Hagai, Y. Levy, Ubiquitin not only serves as a tag but also assists degradation by inducing protein unfolding. *Proc. Natl. Acad. Sci. U.S.A.* **107**, 2001–2006 (2010).
20. Y. Gavrilov, T. Hagai, Y. Levy, Nonspecific yet decisive: Ubiquitination can affect the native-state dynamics of the modified protein. *Protein Sci.* **24**, 1580–1592 (2015).
21. E. C. Carroll, E. R. Greene, A. Martin, S. Marqusee, Site-specific ubiquitination affects protein energetics and proteasomal degradation. *Nat. Chem. Biol.* **16**, 866–875 (2020).
22. D. Morimoto, E. Walinda, H. Fukada, K. Sugase, M. Shirakawa, Ubiquitylation directly induces fold destabilization of proteins. *Sci. Rep.* **6**, 39453 (2016).
23. A. Ciechanover, A. L. Schwartz, The ubiquitin system: Pathogenesis of human diseases and drug targeting. *Biochim. Biophys. Acta* **1695**, 3–17 (2004).
24. D. Senft, J. Qi, Z. A. Ronai, Ubiquitin ligases in oncogenic transformation and cancer therapy. *Nat. Rev. Cancer* **18**, 69–88 (2018).
25. L. Wang *et al.*, Host-mediated ubiquitination of a mycobacterial protein suppresses immunity. *Nature* **577**, 682–688 (2020).
26. M. J. Lubienski, M. Bycroft, D. N. M. Jones, A. R. Fersht, Assignment of the backbone 1H and 15N NMR resonances and secondary structure characterization of barstar. *FEBS Lett.* **332**, 81–87 (1993).
27. M. J. Lubienski, M. Bycroft, S. M. Freund, A. R. Fersht, Three-dimensional solution structure and 13C assignments of barstar using nuclear magnetic resonance spectroscopy. *Biochemistry* **33**, 8866–8877 (1994).
28. Y. Bai, J. S. Milne, L. Mayne, S. W. Englander, Primary structure effects on peptide group hydrogen exchange. *Proteins* **17**, 75–86 (1993).
29. G. P. Connelly, Y. Bai, M.-F. Jeng, S. W. Englander, Isotope effects in peptide group hydrogen exchange. *Proteins* **17**, 87–92 (1993).
30. Y.-Z. Zhang, "Protein and peptide structure and interactions studied by hydrogen exchange and NMR," PhD thesis, University of Pennsylvania, Philadelphia, PA (1995).
31. S. E. Jackson, Ubiquitin: A small protein folding paradigm. *Org. Biomol. Chem.* **4**, 1845–1853 (2006).
32. A. C. D. Fuchs, L. Maldoner, M. Wojtynek, M. D. Hartmann, J. Martin, Rpn11-mediated ubiquitin processing in an ancestral archaeal ubiquitination system. *Nat. Commun.* **9**, 2696 (2018).
33. Y. Sato *et al.*, Structural basis for specific cleavage of Lys 63-linked polyubiquitin chains. *Nature* **455**, 358–362 (2008).
34. R. K. Shrestha *et al.*, Insights into the mechanism of deubiquitination by JAMM deubiquitinases from cocrystal structures of the enzyme with the substrate and product. *Biochemistry* **53**, 3199–3217 (2014).
35. E. J. Worden, K. C. Dong, A. Martin, An AAA motor-driven mechanical switch in Rpn11 controls deubiquitination at the 26S proteasome. *Mol. Cell* **67**, 799–811.e8 (2017).
36. Y. Ye *et al.*, Polyubiquitin binding and cross-reactivity in the USP domain deubiquitinase USP21. *EMBO Rep.* **12**, 350–357 (2011).
37. K. E. Sloper-Mould, J. C. Jemc, C. M. Pickart, L. Hicke, Distinct functional surface regions on ubiquitin. *J. Biol. Chem.* **276**, 30483–30489 (2001).
38. K. N. Swatek *et al.*, Insights into ubiquitin chain architecture using Ub-clipping. *Nature* **572**, 533–537 (2019).
39. C. Park, S. Marqusee, Probing the high energy states in proteins by proteolysis. *J. Mol. Biol.* **343**, 1467–1476 (2004).
40. C. Park, Probing transient partial unfolding in proteins by native-state proteolysis. *Bio Des.* **2**, 117–128 (2014).
41. D. Balchin, M. Hayer-Hartl, F. U. Hartl, In vivo aspects of protein folding and quality control. *Science* **353**, aac4354 (2016).
42. T. R. Jahn, S. E. Radford, Folding versus aggregation: Polypeptide conformations on competing pathways. *Arch. Biochem. Biophys.* **469**, 100–117 (2008).
43. Y. E. Kim, M. S. Hipp, A. Bracher, M. Hayer-Hartl, F. Ulrich Hartl, Molecular chaperone functions in protein folding and proteostasis. *Annu. Rev. Biochem.* **82**, 323–355 (2013).
44. J. Tyedmers, A. Mogk, B. Bukau, Cellular strategies for controlling protein aggregation. *Nat. Rev. Mol. Cell Biol.* **11**, 777–788 (2010).
45. R. Cliffe *et al.*, Filamentous aggregates are fragmented by the proteasome holoenzyme. *Cell Rep.* **26**, 2140–2149.e3 (2019).
46. Q. Guo *et al.*, In situ structure of neuronal C9orf72 poly-GA aggregates reveals proteasome recruitment. *Cell* **172**, 696–705.e12 (2018).
47. Y. Ye, D. Klenerman, D. Finley, N-terminal ubiquitination of amyloidogenic proteins triggers removal of their oligomers by the proteasome holoenzyme. *J. Mol. Biol.* **432**, 585–596 (2020).
48. A. Zuin, M. Isasa, B. Crosas, Ubiquitin signaling: Extreme conservation as a source of diversity. *Cells* **3**, 690–701 (2014).
49. B. P. Roscoe, K. M. Thayer, K. B. Zeldovich, D. Fushman, D. N. A. Bolon, Analyses of the effects of all ubiquitin point mutants on yeast growth rate. *J. Mol. Biol.* **425**, 1363–1377 (2013).
50. D. Mavor *et al.*, Extending chemical perturbations of the ubiquitin fitness landscape in a classroom setting reveals new constraints on sequence tolerance. *Biol. Open* **7**, bio036103 (2018).
51. F. Mortensen *et al.*, Role of ubiquitin and the HPV E6 oncoprotein in E6AP-mediated ubiquitination. *Proc. Natl. Acad. Sci. U.S.A.* **112**, 9872–9877 (2015).
52. G. T. Debelouchina, K. Gerecht, T. W. Muir, Ubiquitin utilizes an acidic surface patch to alter chromatin structure. *Nat. Chem. Biol.* **13**, 105–110 (2017).
53. P. D. L. Rios, P. Goloubinoff, Hsp70 chaperones use ATP to remodel native protein oligomers and stable aggregates by entropic pulling. *Nat. Struct. Mol. Biol.* **23**, 9–12 (2016).
54. R. Sousa, E. M. Lafer, The physics of entropic pulling: A novel model for the Hsp70 motor mechanism. *Int. J. Mol. Sci.* **20**, 2334 (2019).
55. N. D. Keul *et al.*, The entropic force generated by intrinsically disordered segments tunes protein function. *Nature* **563**, 584–588 (2018).
56. J. A. Caro *et al.*, Entropy in molecular recognition by proteins. *Proc. Natl. Acad. Sci. U.S.A.* **114**, 6563–6568 (2017).
57. S. Dagan *et al.*, Stabilization of a protein conferred by an increase in folded state entropy. *Proc. Natl. Acad. Sci. U.S.A.* **110**, 10628–10633 (2013).

58. K. A. Ball *et al*., Non-degradative ubiquitination of protein kinases. *PLOS Comput. Biol.* **12**, e1004898 (2016).
59. J. M. Gendron *et al*., Using the ubiquitin-modified proteome to monitor distinct and spatially restricted protein homeostasis dysfunction. *Mol. Cell. Proteomics* **15**, 2576–2593 (2016).
60. X. Sun *et al*., PROTACs: Great opportunities for academia and industry. *Signal Transduct. Target. Ther.* **4**, 64 (2019).
61. N. Shabek *et al*., The size of the proteasomal substrate determines whether its degradation will be mediated by mono- or polyubiquitylation. *Mol. Cell* **48**, 87–97 (2012).
62. D. Shental-Bechor, Y. Levy, Effect of glycosylation on protein folding: A close look at thermodynamic stabilization. *Proc. Natl. Acad. Sci. U.S.A.* **105**, 8256–8261 (2008).
63. D. Shental-Bechor, Y. Levy, Folding of glycoproteins: Toward understanding the biophysics of the glycosylation code. *Curr. Opin. Struct. Biol.* **19**, 524–533 (2009).
64. P. Schanda, B. Brutscher, Very fast two-dimensional NMR spectroscopy for real-time investigation of dynamic events in proteins on the time scale of seconds. *J. Am. Chem. Soc.* **127**, 8014–8015 (2005).
65. P. Schanda, H. Van Melckebeke, B. Brutscher, Speeding up three-dimensional protein NMR experiments to a few minutes. *J. Am. Chem. Soc.* **128**, 9042–9043 (2006).
66. E. Lescop, P. Schanda, B. Brutscher, A set of BEST triple-resonance experiments for time-optimized protein resonance assignment. *J. Magn. Reson.* **187**, 163–169 (2007).
67. F. Delaglio *et al*., NMRPipe: A multidimensional spectral processing system based on UNIX pipes. *J. Biomol. NMR* **6**, 277–293 (1995).
68. R. Keller, The computer aided resonance assignment tutorial. http://cara.nmr.ch/doku.php/cara_downloads. Accessed 5 March 2021.
69. R. A. Harrison *et al*., Structural dynamics in ras and related proteins upon nucleotide switching. *J. Mol. Biol.* **428**, 4723–4735 (2016).
70. S. Vijay-Kumar, C. E. Bugg, W. J. Cook, Structure of ubiquitin refined at 1.8 A resolution. *J. Mol. Biol.* **194**, 531–544 (1987).
71. D. A. Case *et al*., AMBER 2019 (University of California, San Francisco, CA, 2019).
72. R. Betz, Dabble. https:/doi.org/10.5281/zenodo.836913. Accessed 1 February 2020.
73. J. A. Maier *et al*., ff14SB: Improving the accuracy of protein side chain and backbone parameters from ff99SB. *J. Chem. Theory Comput.* **11**, 3696–3713 (2015).
74. P. Li, L. F. Song, K. M. Merz Jr, Systematic parameterization of monovalent ions employing the nonbonded model. *J. Chem. Theory Comput.* **11**, 1645–1657 (2015).
75. S. Piana, A. G. Donchev, P. Robustelli, D. E. Shaw, Water dispersion interactions strongly influence simulated structural properties of disordered protein states. *J. Phys. Chem. B* **119**, 5113–5123 (2015).
76. R. Salomon-Ferrer, A. W. Götz, D. Poole, S. Le Grand, R. C. Walker, Routine microsecond molecular dynamics simulations with AMBER on GPUs. 2. Explicit solvent particle mesh ewald. *J. Chem. Theory Comput.* **9**, 3878–3888 (2013).
77. B. A. Chapman, J. T. Chang, Biopython: Python tools for computational biology. *ACM SIGBIO Newsl.* **20**, 15–19 (2000).
78. W. Kabsch, C. Sander, Dictionary of protein secondary structure: Pattern recognition of hydrogen-bonded and geometrical features. *Biopolymers* **22**, 2577–2637 (1983).
79. M. F. Sanner, A. J. Olson, J. C. Spehner, Reduced surface: An efficient way to compute molecular surfaces. *Biopolymers* **38**, 305–320 (1996).